metals

MDPI

Article

Complete Extraction of Amorphous Aluminosilicate from Coal Fly Ash by Alkali Leaching under Atmospheric Pressure

Andrei Shoppert [1,*], Dmitry Valeev [2], Irina Loginova [1] and Leonid Chaikin [1]

[1] Department of Non-Ferrous Metals Metallurgy, Ural Federal University, 620002 Yekaterinburg, Russia; loginova_irina@mail.ru (I.L.); l.i.chaikin@urfu.ru (L.C.)

[2] Laboratory of Sorption Methods, Vernadsky Institute of Geochemistry and Analytical Chemistry of the Russian Academy of Sciences, 119334 Moscow, Russia; dmvaleev@yandex.ru

* Correspondence: a.a.shoppert@urfu.ru

Received: 24 November 2020; Accepted: 16 December 2020; Published: 16 December 2020

Abstract: One of the potential sources of alumina and mesoporous silica is the coal-fired thermal plants waste known as the coal fly ash (CFA). The studies of the alumina extraction from CFA are often focused on the preliminary desilication, but the efficiency of the alkali desilication is low due to formation of the desilication product—$Na_6[Al_6Si_6O_{24}]\cdot Na_2X$ (DSP). This research is focused on the possibility of CFA desilication without formation of DSP using a leaching process with higher liquid to solid ratios (L/S) and alkali concentrations. The experimental data were analyzed using an artificial neural network (ANN) machine learning method and a shrinking core model (SCM). The investigation of the CFA morphology, chemical and phase composition before and after leaching were carried out by scanning electron microscopy with energy-dispersive X-ray spectroscopy (SEM-EDX), inductively coupled plasma optical emission spectrometry (ICP-OES) and X-ray diffraction (XRD). The present work shows that it is possible to avoid formation of DSP if using the L/S ratio >20 and concentration of Na_2O—400 g/L during CFA leaching. The kinetics analysis by SCM showed that the process is limited by the surface chemical reaction at T <100 °C, and by diffusion through the product layer at T >100 °C, respectively. The SEM images of the solid residue after NaOH leaching under conditions that prevent the DSP formation show mullite particles with an acicular structure.

Keywords: coal fly ash (CFA); amorphous aluminosilicate; desilication; alkali leaching; acicular mullite; neural network; kinetics; shrinking core model

1. Introduction

Coal is the main source of energy worldwide. The ever-increasing energy demand means that coal will remain a key component in energy generation for the nearest future [1], with proven reserves of over 1000 billion tons [2]. As a result of coal combustion on thermal power plants (TTP), the solid residue is formed, which is usually referred to as coal fly ash (CFA). The CFA content of most coals is around 10–20%, while it reaches ~40% in the brown coal from the Ekibastuz basin of Kazakhstan Republic [3]. The volume of generated CFA will increase in upcoming years due to the increasing need for energy from coal plants. The degree of CFA utilization is also increasing, but it still does not exceed 70% in China, USA and India, etc. Moreover, the average utilization rate in the world, according to various estimates, is not more than 25% [4,5], and there is a large difference between developed and developing countries.

In Russia, over 90 million tons of coal was combusted in 2018 to generate electricity [6]. This value corresponds to 25 million tons of CFA [7], while the CFA utilization rate was less than 8.5% [8]. A total

of 1.5 billion tons of CFA has been accumulated in Russian ash landfills. At many TPPs, the capacity of ash landfills for storing new amounts of ash is practically exhausted. Damage caused by CFA to the environment includes pollution of soil and groundwater by the natural leaching of heavy metals from CFA as well as risk of chronic lung diseases for people living close to the ash landfills [9].

CFA contains a large number of valuable components, and its recycling can be economically and environmentally beneficial. In China, great efforts have been made to develop efficient ways of utilizing CFA [10,11]. About 20% of the generated CFA is used for production of concrete [2]. Other areas include land reclamation [12–14], ceramic industry [15–18], production of catalysts [19–22], sorbents [23], deep separation of useful components [24–27], zeolites [28–31] and extraction of non-ferrous metals [32–35].

The chemical composition of CFA depends on the combustion method and coal deposit [10]. In the province of Inner Mongolia in China, CFA with high alumina (Al_2O_3) content is formed, up to 50 wt.% [35]. The alumina content in Russian CFA is not more than 25–30 wt.% and it contains more than 60% of silica (SiO_2). This fact reduces the economic attractiveness of the Russian CFA for sandy grade alumina production [36], since a preliminary removal of silicon from the CFA is necessary. The choice of a method depends on the minerals where alumina and silica are concentrated. The phase composition of CFA depends mainly on the method of coal combustion. If heat boilers are used in TPP with the combustion temperature above 1300 °C, the main alumina-containing mineral is mullite ($Al_6Si_2O_{13}$) [37], while in the CFA obtained in fluidized bed combustion, most of Al_2O_3 is concentrated in an amorphous glassy residue [38].

The main method for desilication of CFA is leaching by caustic alkali solution (NaOH). Silica can easily be leached at atmospheric pressure from an amorphous glassy mass. This type of leaching produces a silicate solution that can be used to precipitate mesoporous silica [39]. The desilication degree by this method does not exceed 60% [40–45] because of the simultaneous process of Al leaching and the precipitation of an insoluble compound—desilication product (DSP) [46]. This process can be described by the following Equations (1–2):

$$x\mathrm{Al_2O_3}\cdot y\mathrm{SiO_2}(\text{amorphous}) + 2(x+y)\mathrm{NaOH} \rightarrow y\mathrm{Na_2SiO_3} + 2x\mathrm{NaAl(OH)_4} + (y-3x)\mathrm{H_2O}, \quad (1)$$

$$6\mathrm{Na_2SiO_3} + 6\mathrm{NaAl(OH)_4} + \mathrm{Na_2}X \rightarrow \mathrm{Na_6[Al_6Si_6O_{24}]}\cdot\mathrm{Na_2}X + 12\mathrm{NaOH} + 6\mathrm{H_2O}, \quad (2)$$

where X represents various inorganic anions, most often sulfate, carbonate, chloride, aluminate, etc.

The formation of a DSP as a result of alkaline leaching of fly ash has been used in many studies to produce zeolites [47,48]. However, large amounts of SiO_2 and Na_2O are lost with the solid residue, if the main goal is to further alumina extraction from this residue. The Na_2O content in the solid residue after conventional leaching reaches 12 wt.%. To reduce alkali losses it was proposed to use preliminary extraction of soluble alumina by acid leaching [49]. Ma et al. [38] showed that by using dual treatment of CFA by acid and alkali, the silica extraction degree reaches only 70%. Leaching of silica from the surface of the CFA particles allows for destruction of the Si-O-Al bonds. The alumina extraction degree significantly increases from 40% to 85% during subsequent acid leaching. This fact is related to formation of DSP readily leached in HCl by Equation (3).

$$\mathrm{Na_6[Al_6Si_6O_{24}]}\cdot\mathrm{Na_2}X + 24\mathrm{HCl} \rightarrow 6\mathrm{AlCl_3} + 6\mathrm{NaCl} + \mathrm{Na_2}X + 12\mathrm{H_2O} + 6\mathrm{SiO_2}. \quad (3)$$

In the previous studies devoted to bauxite [50,51], it was found that under certain conditions it is possible to keep alumina and silica in liquor for a long time without the formation of DSP. This made it possible to obtain red mud with high iron content. This opportunity appears mainly by the leaching of sodium aluminate containing sintering products under atmospheric pressure with highly concentrated NaOH solutions. In these conditions, the limited solubility of silica is observed. After reaching supersaturation, regardless of liquor temperature, DSP formation begins.

The main purpose of this study is to show the possibility of increasing the SiO_2 extraction degree from CFA by NaOH leaching while reducing the loss of NaOH with solid residue by keeping Al_2O_3 in

the liquor. In addition, to analyze the influence of technological parameters on the CFA desilication degree and create a process model in this research, we used neural networks. For determination of the mechanism interaction of CFA with NaOH, the kinetics of the leaching process using a shrinking core model was studied.

2. Materials and Methods

2.1. Analysis

Mineralogy of the raw CFA and the samples after alkali leaching were measured by X-ray diffraction (XRD) using a Difrei-401 diffractometer (JSC Scientific Instruments, Saint Petersburg, Russia) using a Cr-Kα radiation source and a 2θ range from 15° to 140° with 30 min exposure time. The operating mode of the X-ray source was set to 25 kW/4 mA. The mineral phases were analyzed by Match 3 software.

The chemical composition of CFA and solid residue was measured by inductively coupled plasma optical emission spectrometry (ICP-OES) at an atomic absorption spectrometer, Varian AA-240FS (Agilent Technologies, San Jose, CA, USA). For quality assurance, samples were analyzed twice. The carbon contents were determined by a fractional gas analyzer, CS-600 (LECO Corporation, St. Joseph, CA, USA).

The surface morphology and elemental composition of the raw CFA and the samples after NaOH leaching were investigated by scanning electron microscopy with energy-dispersive X-ray spectroscopy (SEM-EDX, Vega III, Tescan, Brno, Czech Republic).

The average particle size and specific surface area of the CFA samples were determined by laser diffraction method (LD) using an Analysette 22 NanoTec (Fritsch, Idar-Oberstein, Germany) and by the Brunauer–Emmett–Teller method (BET) using NOVA 1200e (Quantachrome Instruments, FL, USA), respectively. Before sorption analysis, all samples were subjected to degassing under vacuum at 200 °C for 12 h.

2.2. Experiments

CFA leaching by NaOH was carried out in an apparatus consisting of a 0.5 L stainless steel reactor, with openings for injecting chemical reagents, as well as for temperature control and the recycling of evaporated water through a water-cooled reflux condenser. The reactor was thermostated. The materials were stirred using an overhead mixer at 700 rpm (if not stated otherwise), which ensured uniform density of the pulp. A predetermined portion of the CFA was added to a prepared alkali solution with the concentration of 400 g/L Na_2O. At the end of the experiment, the leaching pulp was filtered in a Buchner funnel; the leaching cake was washed with distilled water, dried at 100 °C for 240 min, weighed and analyzed by ICP-OES. All the experiments were performed twice and the mean values are presented here. The loss on ignition (LOI) was determined by calcination at 1000 °C for 60 min.

2.3. Materials and Reagents

The CFA formed from combustion of Ekibastuz brown coal at the Reftinskaya thermal power plant in Asbest, Russia was used as a raw material. The particle size distribution of the raw CFA is shown in Figure 1. A part of the CFA used in the kinetic study was additionally grinded and subjected to sieve analysis to obtain three size fractions with a similar chemical composition: −50 μm, +50–74 μm and +74 μm. The mean content of oxides and elements of CFA is shown in Table 1.

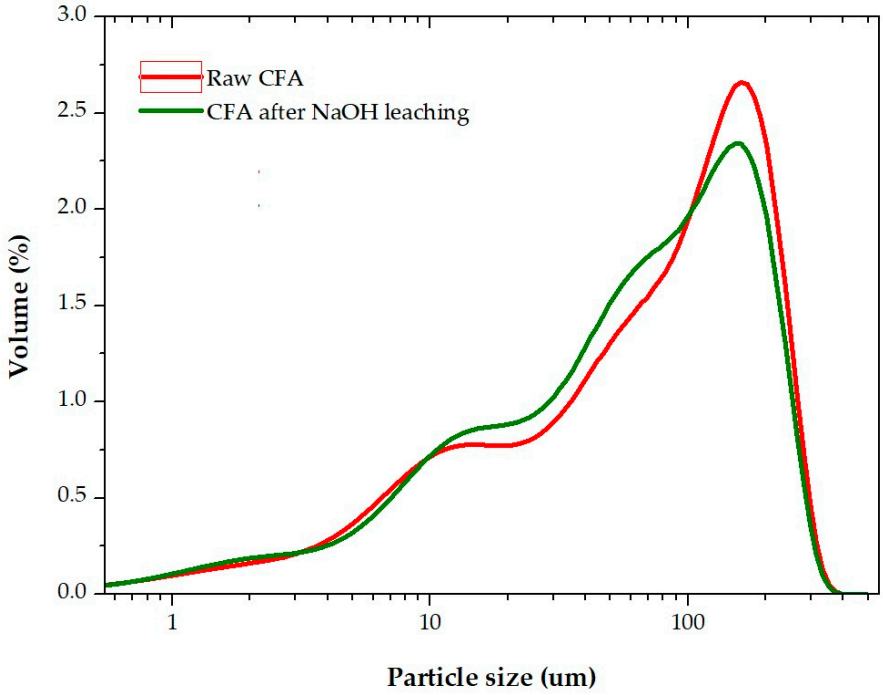

Figure 1. The particle size distribution of the raw coal fly ash (CFA) and CFA after NaOH leaching at T = 110 °C, liquid to solid (L/S) ratio = 21.5, τ = 75 min.

Table 1. Chemical composition of the CFA from Reftinskaya thermal power plant (TPP), Asbest, Russia.

Main Components, wt.%									
SiO_2	Al_2O_3	CaO	Fe_2O_3	TiO_2	MgO	Na_2O	K_2O	LOI	C
63.12	23.40	1.85	4.85	1.17	0.51	0.75	0.59	3.99	1.60

Figure 2 shows the XRD analysis of the raw CFA. It can be seen that the raw CFA mainly consists of three mineral phases: mullite, magnetite (Fe_3O_4), quartz (SiO_2) and a high amount of a glassy amorphous phase (from 20 to 40 degrees on Figure 2). The amorphous phase (A-S), in addition to mullite, also could contain potassium (K-A-S) and calcium feldspars (Ca-A-S), which are found in the SEM image (Figure 3, Table 2), but are not seen in XRD pattern due to the small amount, low crystallinity and relatively close peaks position with quartz. The quantitative analysis of amorphous and crystalline phases in the CFA sample was carried out by the method used in the Abdrakhimov et al. article [52] (Table 3). It combines the Rietveld method and the complete removal of the glassy amorphous phase. The SEM images in Figure 3 also demonstrate that mullite and magnetite particles are predominantly spherical in shape with a relatively smooth surface, while amorphous particles have an irregular shape with a rough surface. It can be seen in Figure 3b that the surface of mullite particles is covered by a glassy amorphous phase.

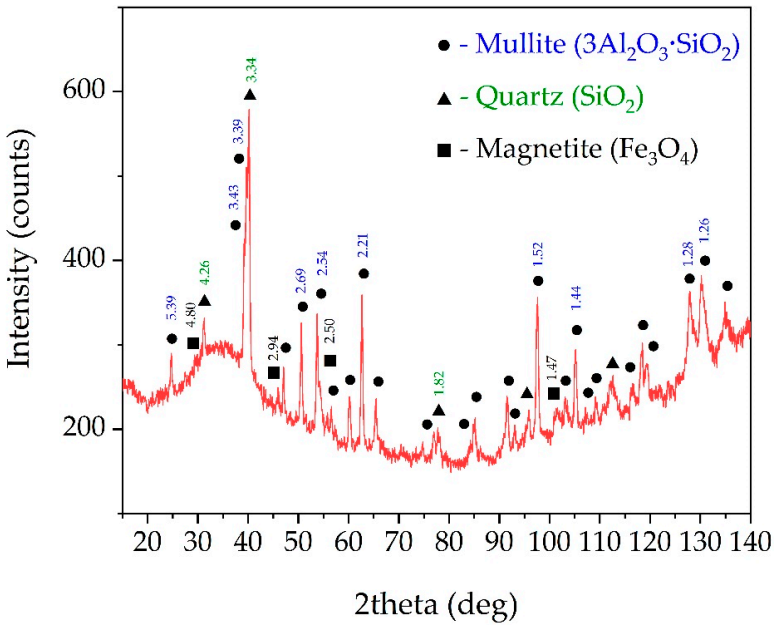

Figure 2. X-ray diffraction (XRD) patterns of the raw CFA from Reftinskaya TPP, Asbest, Russia (the numbers above the peaks refer to *d*-spacing).

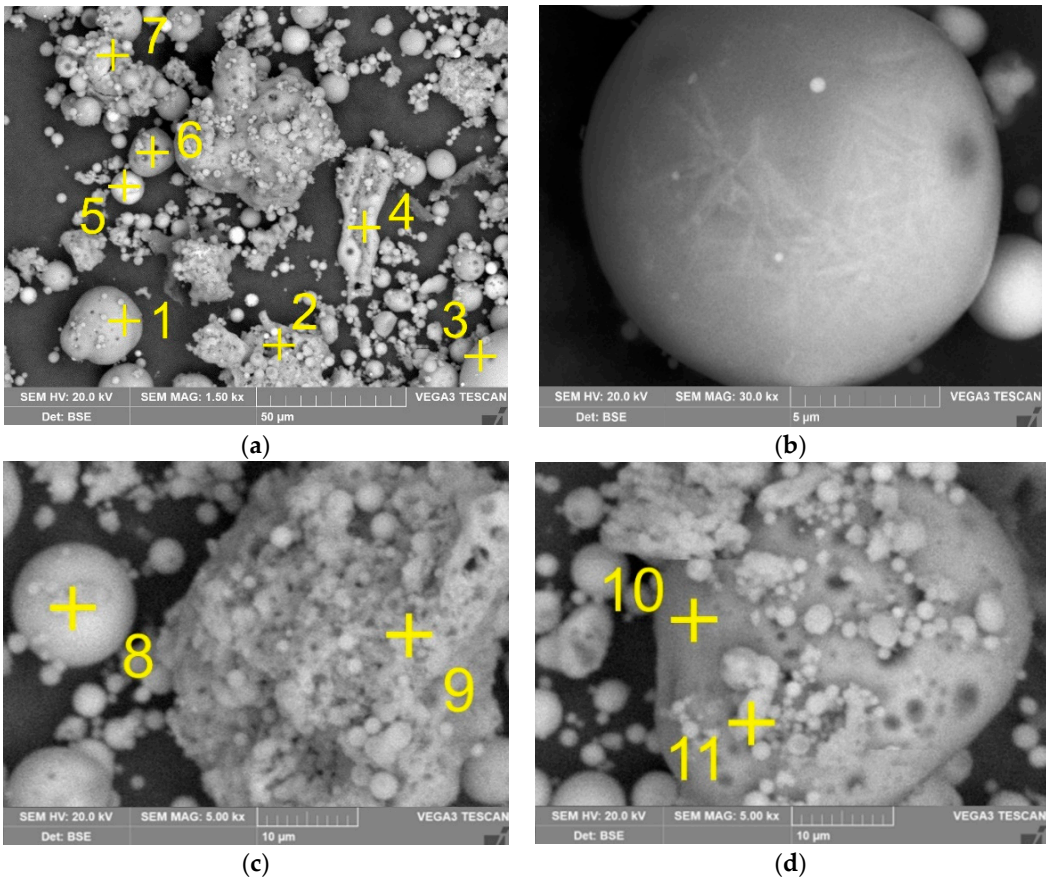

Figure 3. The SEM images of raw CFA at magnitude 1500 (**a**) mullite particles covered by amorphous aluminosilicate (A-S) at magnitude 30,000 (**b**) and at magnitude 5000 (**c**,**d**) (yellow cross indicates place of scanning electron microscopy with energy-dispersive X-ray spectroscopy (SEM-EDX) analysis; the elemental compositions are shown in Table 2).

Table 2. The elemental compositions (wt.%) of CFA particles (see Figure 3 for the spectra numbers).

Spectrum	O	Si	Al	Ca	K	Fe	Ti	Mg	Na	Phase
1	53.9	20.5	16.5	1.0	1.1	6.1	0.3	-	0.7	Mullite + A-S [1]
2	52.9	30.4	14.7	0.3	0.7	0.3	0.3	-	0.5	A-S
3	46.1	22.7	4.8	4.6	-	19.2	0.8	1.7	-	Magnetite + Ca-A-S [2]
4	52.7	26.0	10.6	0.3	0.8	8.0	-	0.7	0.5	A-S
5	56.1	8.2	5.8	0.7	-	0.7	19.7	0.2	0.2	Rutile + A-S
6	54.2	22.7	21.3	-	0.5	0.4	0.4	-	0.6	Mullite + A-S
7	56.3	9.8	4.6	11.6	-	0.3	-	0.3	-	Ca-A-S
8	57.5	21.6	9.8	8.4	0.3	1.3	-	-	0.4	Ca-A-S
9	57.2	31.1	10.6	-	0.8	-	0.4	-	-	A-S
10	50.8	26.5	18.8	0.7	0.7	1.2	0.5	0.4	0.5	Mullite + A-S
11	59.2	23.7	14.6	0.3	0.5	1.1	-	-	0.6	A-S

[1] A-S—amorphous aluminosilicate; [2] Ca-A-S—Ca containing amorphous aluminosilicate.

Table 3. Semi-quantitative determination of mineral phases in raw CFA.

Phase	Content %
Amorphous	50.26
Mullite	22.05
Quartz	12.06
Feldspar	7.22
Magnetite	4.69
Rutile	1.17
Other	2.55
Total	100

Other materials used in the present research include: caustic alkali of the reagent grade (JSC Soda, Sterlitamak, Russia) and distilled water.

3. Results and Discussion

3.1. The Effect of Leaching Conditions on the Desilication Efficiency

In this research, the possibility of CFA leaching by highly concentrated alkaline solutions (HCAS) at an increased liquid to solid (L/S) ratio and atmospheric pressure was investigated. This method allows excluding the DSP formation. The application of HCAS allows using temperatures above 100 °C without high-pressure equipment. The boiling point of a solution with a concentration of 430 g/L NaOH (32%) or 330 g/L Na_2O is 120 °C. To reduce the number of experiments and to identify the mutual influence of various factors on each other, a full factorial design method was used. The matrix of experiments and the results obtained on the extraction of aluminum and silicon into solution, as well as the Na_2O content in the solid residue are shown in Table 4. The concentration of caustic alkali in all experiments was 400 g/L Na_2O to exclude solution boiling at high temperatures.

Xie et al. and Shokri [53,54] showed that the use of machine learning provides more accurate models than traditional mathematical methods. The results obtained for the Si and Al extraction into liquor and the Na_2O content in the solid residue that are given in Table 4 were analyzed using machine learning with artificial neural networks (ANNs) included in the "Statistica 13" software. The best results were obtained by the architecture MLP (a multilayer perceptron) 3-8-3, where the first digit is the number of input neurons, the second is the number of hidden neurons, and the last is the number of output neurons. High convergence of experimental data and values predicted using the resulting network is obtained (R^2 = 0.97). The response surfaces predicted by the ANN for extracting Si and Al into liquor, as well as the Na_2O content in the solid residue, depending on the duration and the L/S ratio at the T = 110 °C are shown in Figure 4. To obtain more exact results, the network was additionally trained using experimental data of the leaching kinetics presented in Section 3.2.

Table 4. The matrix for planning experiments and the results obtained on the leaching of aluminum and silicon into liquor and the sodium content in the solid residue of CFA.

No.	Time (min)	L/S Ratio (mL/g)	Temperature (°C)	Si Recovery (%)	Al Recovery (%)	Na_2O in Solid Residue (%)
1	30	10	120	76.82	17.99	6.00
2	120	20	120	79.54	29.35	10.12
3	120	20	100	77.24	20.74	3.02
4	75	21.5	110	91.63	41.64	0.89
5	30	20	100	52.13	6.38	0.44
6	75	15	110	70.26	5.86	8.86
7	75	15	97	64.20	18.43	0.46
8	120	10	100	60.57	2.08	7.62
9	120	10	120	56.86	1.00	11.00
10	133	15	110	66.44	5.66	9.99
11	30	20	120	88.14	43.75	0.65
12	75	8.5	110	83.87	40.11	8.05
13	75	15	123	73.87	21.05	10.59
14	75	15	110	69.18	9.50	8.86
15	30	10	100	44.87	12.59	0.53
16	17	15	110	59.06	21.97	0.42

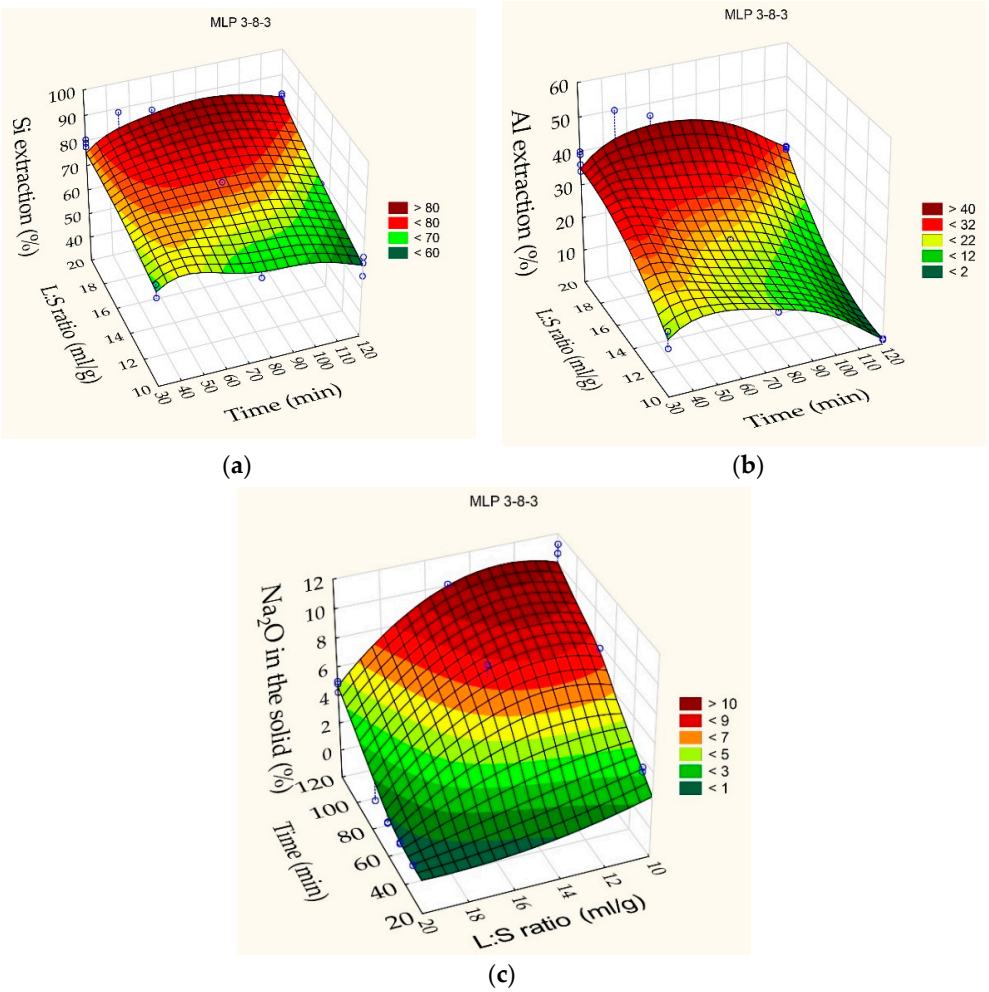

Figure 4. Neural network response surfaces for: (**a**) Si extraction degree in the alkali solution; (**b**) Al extraction in the alkali solution; (**c**) Na_2O content in the solid residue. Blue points are the experimental data.

According to the response, surfaces shown in Figure 4, at the L/S ratio of up to 20 and 60 min duration, the Si and Al extraction degrees were 88% and 45%. A minimum of Na_2O content (0.89 mas.%) is observed in the solid residue at these leaching conditions. It indicates the absence of the DSP formation and maintenance of all readily soluble alumina in liquor. A decrease in L/S ratio to 15-10 allows for a severe increase in the Na_2O content in the solid residue, especially after 120 min leaching duration. This fact indicates the beginning of the DSP formation. At 120 min of leaching duration, the Na_2O content in the solid residue also begins to increase at L/S ratio 20, as the Si and Al extraction degree also begin to decrease. This suggests that the liquor may be in the metastable area [55] until reaching about 90 min (maximum Si extraction degree in Figure 4). The appearance of nuclei or an insignificant increase in the concentration of silica leads to further supersaturation and the beginning of mass precipitation of the DSP—a transition to the labile area.

3.2. Kinetic Study

The influence of various process conditions on the kinetics with the L/S = 20 and Na_2O concentration of 400 g/L was investigated for a detailed understanding of the mechanism of the CFA leaching. The experimental points are shown in Figure 5. The average particle size in all experiments was 62 µm (except for Figure 5b), stirring speed 700 min^{-1} (except for Figure 5c), T = 110 °C (except for Figure 5a).

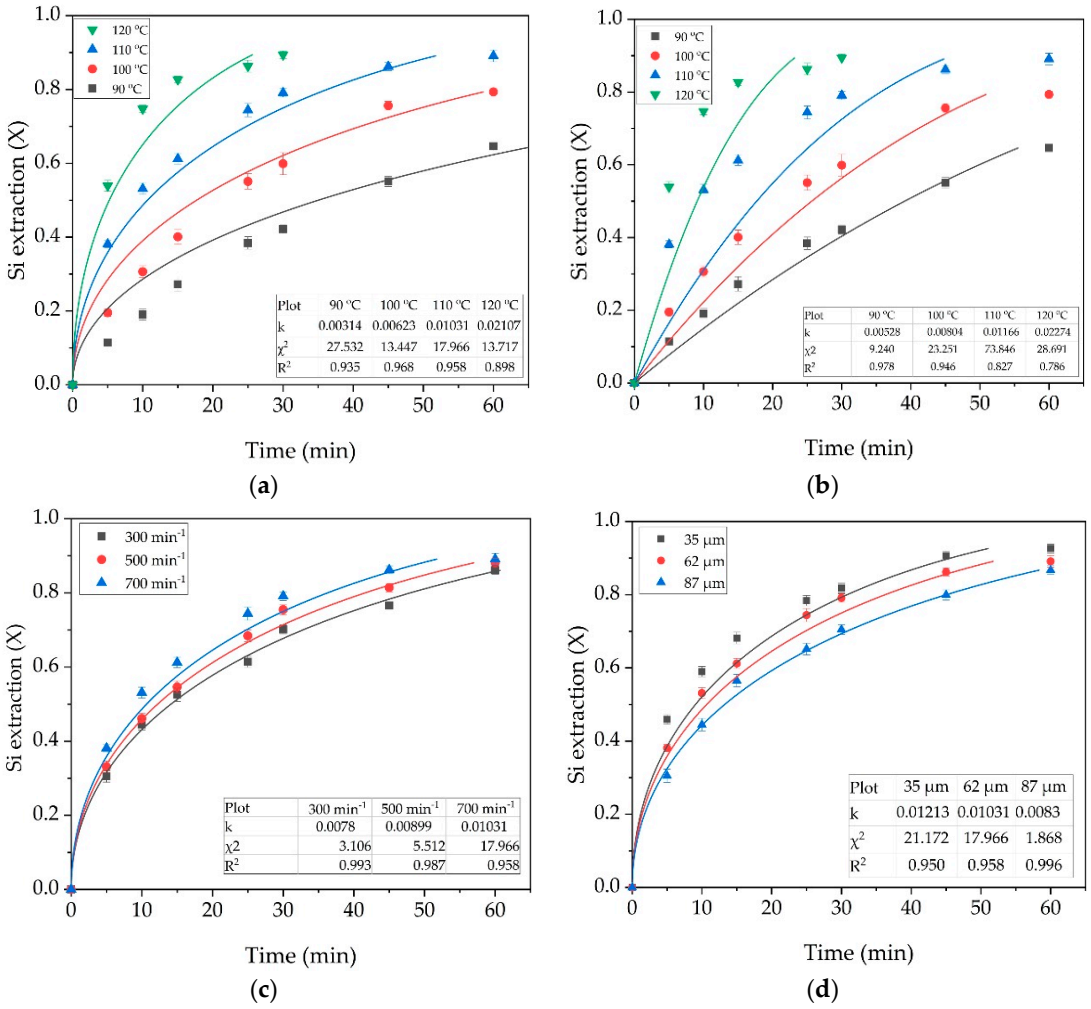

Figure 5. The results of fitting experimental data (points) by the shrinking core model (lines): the diffusion through the liquid film (**a**); the surface reaction for the effect of temperature (**b**); (**c**) the diffusion through the liquid film for the effect of stirrer rate; and (**d**) the diffusion through the liquid film for the average particle size.

The experimental data from Figure 4 were analyzed using various shrinking core models [56]. These models assume that by the leaching of the original particle, its core shrinks towards the center, leaving behind an inert layer of the reaction product. In this case, mullite, quartz, unburned coal and magnetic particles are not leached by NaOH and can be the inert reaction product.

Three model equations were used. When the leaching rate is limited by the surface chemical reaction, the kinetic equation can be written as:

$$[1 - (1 - X)^{1/3}] = k_1 t, \quad (4)$$

where X is the degree of conversion; k_i is the apparent rate constant; t is the leaching time, min.

If the leaching kinetic is limited by the diffusion through porous layer of the product, then the following equation can be used:

$$[1 - 2/3X - (1 - X)^{2/3}] = k_2 t. \quad (5)$$

When the leaching rate is limited by the diffusion through the liquid film (external diffusion), the kinetic equation can be transformed into:

$$X = k_3 t. \quad (6)$$

All the kinetic parameters and their standard errors were calculated with non-linear least-squares methods using commercial software. The non-linear least-squares method has a large number of advantages over linearization, and one of the main ones is the possibility to evaluate the quality of fitting experimental data by the non-linear chi-square test (χ^2) [57]. The best convergence of the experimental data with the shrinking core model was obtained using Equations (4) and (5).

The data presented in Figure 5a,b show that at temperatures below 100 °C, the kinetic model provides the best fit for the experimental data. However, at temperatures above 100 °C, the model is more suitable for diffusion through the reaction product. At T = 120 °C, complete extraction of amorphous aluminosilicates is quickly reached, which leads to low convergence of the experimental data with the model even without taking into account the points after 30 min of leaching. At high temperatures, the surface reaction proceeds rather quickly and the process rate can be limited by the access of the NaOH to the core through the product layer. The effect of stirring speed (Figure 5c) is not as high as for temperature. This fact can indicate that there are no external diffusion limitations. An increase of the average particle size also has a smaller effect on the kinetics than temperature. Figure 5d shows that the experimental data obtained using larger particles (87 μm) are best suited to the diffusion model through the reaction product (lowest χ^2 value). This observation is in good agreement with the shrinking core model, since when the particle size is larger, so the product layer will be thicker.

The values of reaction rate constants obtained from Figure 5b were used to calculate the apparent energy activation (E_a) and experimental orders of the stirring rate and average particle size by plotting graphs in the coordinates lnk-1000/T, lnk-lnυ and lnk-lnr_o, where k—constant rate on the corresponding graphs in Figure 5; T—process temperature, K; υ—stirring speed, min^{-1}; and r_o is the average particle size, μm. Linear fit (Figure 6) was used to determinate the E_a and the reaction orders according to the Arrhenius equation (7):

$$k = k_0 \exp(-E/RT). \quad (7)$$

where k_0 is the pre-exponential factor; E is the apparent activation energy, kJ/mol; T is the reaction temperature, K; and R is the universal gas constant, 8.314 J/mol·K.

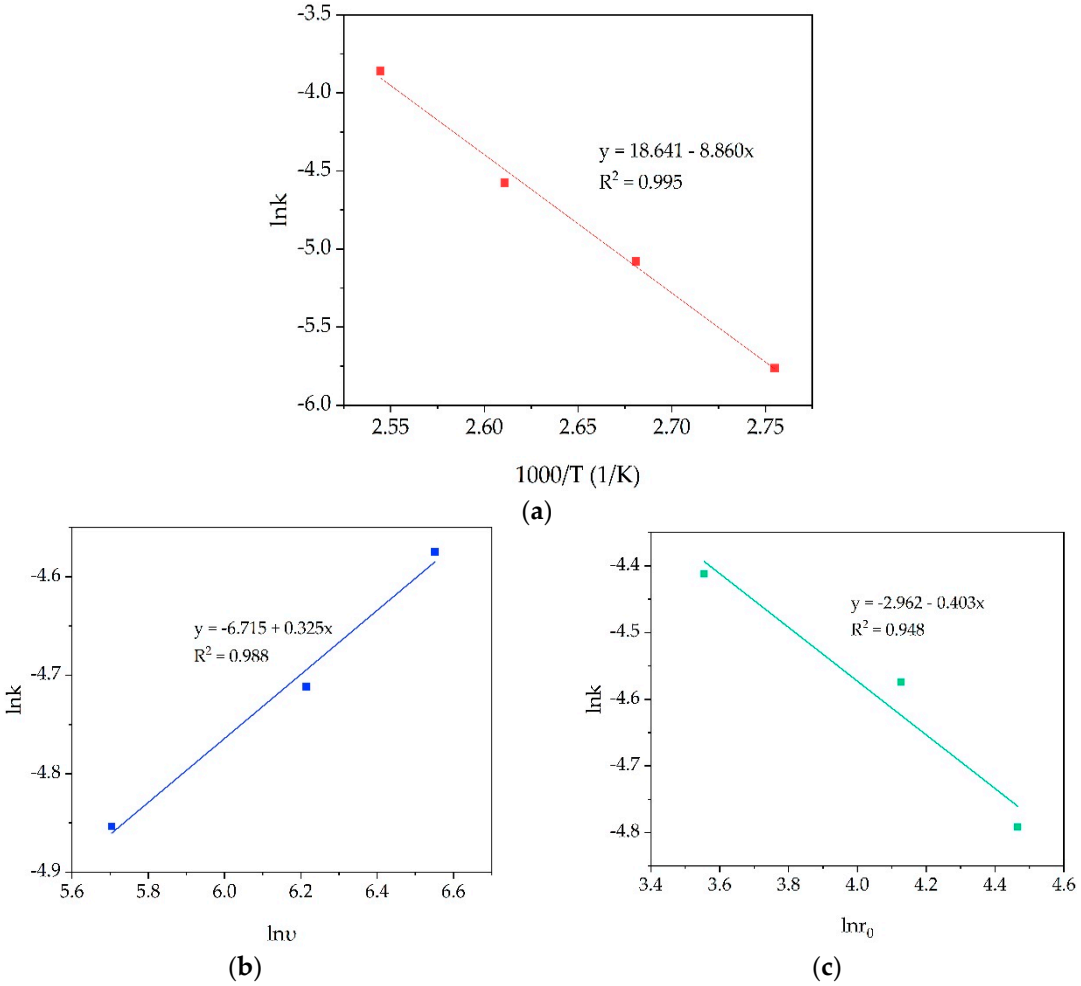

Figure 6. Relationship between lnk–1000/T from Figure 5a (**a**); lnk-lnυ from Figure 5c (**b**); and lnk-lnr$_o$ from Figure 5d (**c**) for CFA desilication by NaOH at L/S ratio = 20:1.

According to the slope obtained in Figure 6a, the E_a value is 73.8 kJ/mol. It confirms that surface chemical reaction is the rate limiting step of the process, especially at T < 100 °C. This fact is due to the need for high activation energy for the leaching of more refractory aluminosilicates at the later stages of the process. The stirring speed order was 0.325, and for the average particle size, this value was 0.403. The obtained low values of orders confirm the absence of serious limitations caused by the diffusion process.

3.3. Solid Residue Characterization

The chemical composition of the solid residue obtained at T = 110 °C, L/S ratio = 21.5 and leaching duration for 75 min (see #4, Table 4) is presented in Table 5. This CFA sample was investigated by XRD and SEM-EDX to identify minerals that react under these conditions. The morphology and porosity of this solid residue were studied as well using the BET method. X-ray diffraction of the solid residue after NaOH leaching (#4 sample) is shown in Figure 7.

Table 5. Chemical composition of the solid residue (#4 from Table 4) after CFA leaching by NaOH.

Main Components, wt.%									
SiO_2	Al_2O_3	CaO	Fe_2O_3	TiO_2	MgO	Na_2O	K_2O	LOI	C
23.42	41.42	2.83	15.30	3.69	1.61	0.89	0.28	8.15	5.05

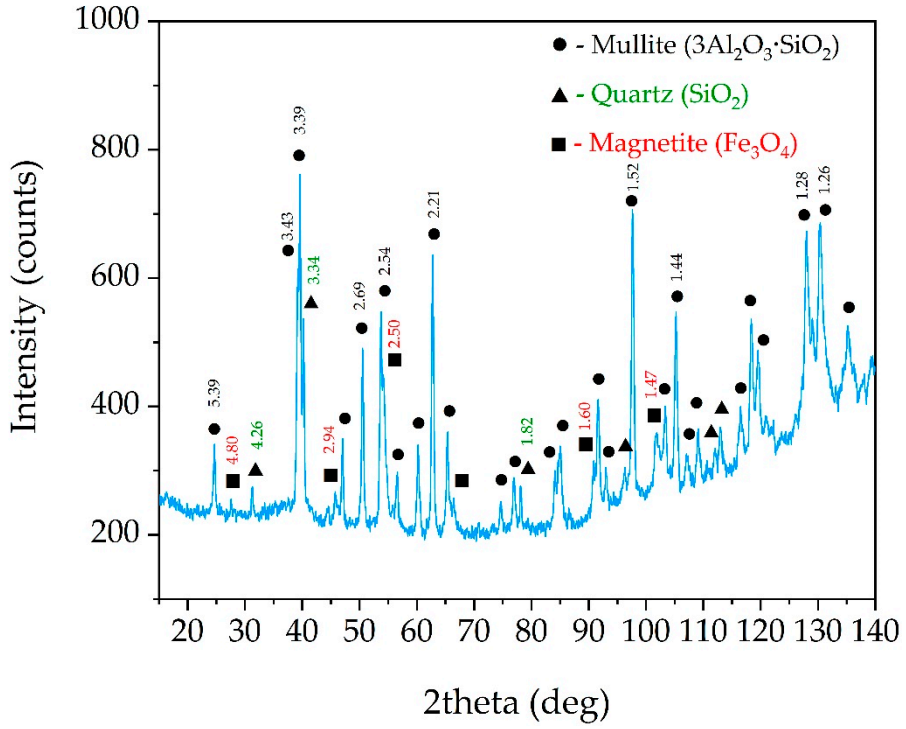

Figure 7. XRD pattern of the solid residue obtained after NaOH leaching at T = 110 °C, L/S ratio = 21.5, τ = 75 min (the numbers above the peaks refer to d-spacing).

As can be seen in Figure 7, the amorphous glassy mass, observed in Figure 2, in the range from 20 to 40 degrees, disappears, while the mullite peaks increase significantly. This fact suggests that amorphous aluminosilicates are predominantly leached out while mullite remains unleached. The peaks of quartz are decreased in comparison with the raw CFA, which indicates that 120 °C and high concentration of sodium alkali is sufficient to dissolve even such a refractory mineral as quartz.

The data obtained are confirmed by the SEM-EDX method (Figure 8 and Table 6). Figure 8a,b show that during the leaching process, at the surface of the raw particles a large number of pores are created, while inside large particles (more than 50 μm), smaller ones are found, access to which is limited. This can be caused by the diffusion limitation at T = 110–120 °C, which is indicated by the results of the shrinking core model (Figure 5). The particles with an acicular structure are shown on the SEM images of the solid residue (Figure 8b). The EDX analysis has been done to clarify their chemical composition.

According to the spectrum in Figure 8c, it can be seen that no glassy amorphous mass is found at the solid residue surface, but a large amount of mullite, magnetite, quartz and unburned coal is left. The elemental composition of mullite particles approaches stoichiometric mullite ($Al_6Si_2O_{13}$). While in the raw CFA (Table 2), the mullite surface was covered with a glassy mass, since the content of SiO_2 was higher in comparison with Al_2O_3. According to EDX analysis (Figure 8d,e), acicular particles were mullite phase. Previous studies have shown that artificial mullite obtained at T >1300 °C may have an acicular structure [58]. The absence of such particles in the raw CFA can be explained by coating of mullite by glassy phase. Such a particle can be seen in Figure 3b, where the same acicular structure is visible under the thin surface layer. Due to the high specific surface area, the mullite particles may sorb the molten glassy mass on the surface during CFA formation.

At the desilication process by NaOH with high L/S ratio, only amorphous glassy mass and quartz are leached and there is no DSP formation comparing with the desilication at low L/S ratio. This leads to the exposure of mullite particles with an acicular structure and an increase in the porosity of the solid residue. Physical characteristics of the raw CFA and the solid residue after alkali leaching are shown in Table 7.

According to the data in Table 7, it can be seen that after desilication the specific surface area of raw CFA significantly increases, despite the similar particle size. The high value of the specific surface area of the solid residue should have a positive effect on the kinetics of the subsequent alumina extraction by HCl leaching.

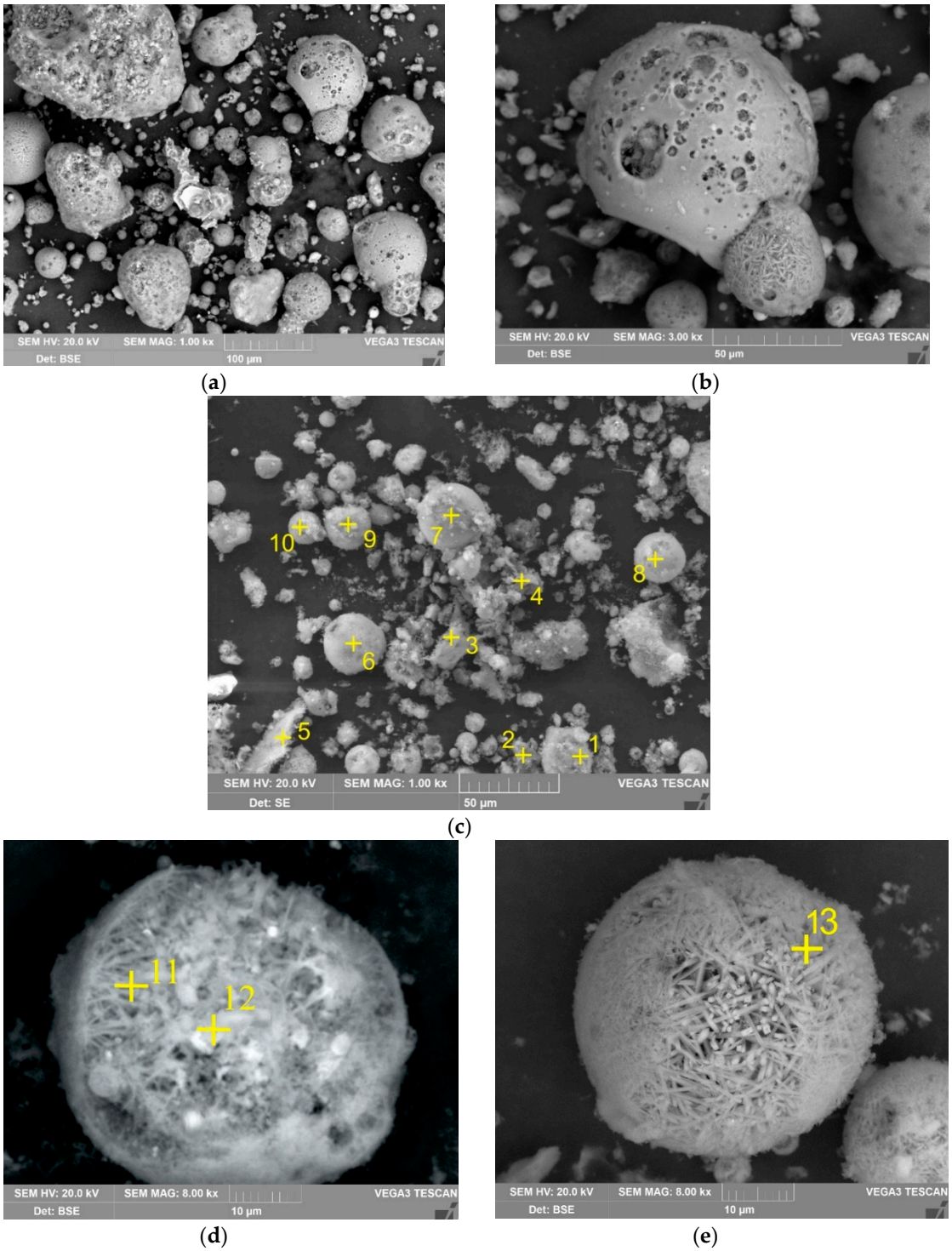

Figure 8. The SEM images of the solid residue at 1000 magnitude (**a**) and at 3000 magnitude (**b**); the SEM images with the EDX analysis at 1000 magnitude (**c**) and at 8000 magnitude (**d**,**e**) (yellow cross indicates place of SEM-EDX analysis; the elemental compositions are shown in Table 6).

Table 6. The elemental compositions (wt.%) of solid residue (see Figure 8 for the spectra numbers).

Spectrum	O	Si	Al	Ca	K	Fe	Ti	Mg	Na	C	Phase
1	40.5	4.2	5.4	15.3	0.3	27.5	1.8	0.6	0.5	-	Magnetite + Ca-A-S
2	61.7	37.5	0.8	-	-	-	-	-	-	-	Quartz
3	23.3	1.9	4.8	0.7	-	0.8	0.7	-	-	67.7	C
4	55.9	30.4	2.7	0.8	-	0.5	0.3	-	0.2	-	Quartz
5	33.2	5.0	14.7	0.2	-	0.4	0.3	-	-	46.2	C + mullite
6	57.1	10.4	30.7	0.3	0.4	0.7	0.5	0.3	0.4	-	Mullite
7	37.6	1.9	8.1	6.2	0.3	44.6	6.2	1.0	-	-	Magnetite + Ca-A-S
8	59.0	10.7	30.2	0.3	-	-	0.5	-	-	-	Mullite
9	52.2	12.0	31.4	0.6	0.4	0.9	1.0	0.5	-	-	Mullite
10	43.0	6.5	24.3	0.4	0.3	0.4	1.7	-	-	23.6	C + mullite
11	65.1	20.5	8.6	3.5	-	0.5	0.6	0.4	-	-	Ca-A-S
12	61.1	10.1	20.0	4.5	-	0.7	1.4	-	-	-	Mullite + Ca-A-S
13	57.9	10.3	30.9	0.2	0.2	0.2	0.3	-	-	-	Mullite

Table 7. The textural properties and particle size of the raw CFA and the solid residue after desilication.

CFA	Specific Surface Area (BET) (m^2/g)	Total Pore Volume (cm^3/g)	Pore Diameter (nm)	Particle Size Distribution (μm)		
				Dx (10)	Dx (50)	Dx (90)
Raw CFA	0.81	0.07	88	7.17	77.06	210.38
Solid residue	15.70	8.99	25	7.41	67.23	200.45

Based on the above research, the mechanism for the desilication process of the raw CFA with the appearance of acicular structure mullite particles is proposed (Figure 9). During the CFA particles formation at T >1300 °C, mullite particles are covered with a glassy amorphous mass, which subsequently solidifies into a film. Due to the NaOH leaching under conditions that prevent the formation of a DSP, mullite particles with an acicular structure are exposed. This leads to a significant increase of the porosity and specific surface area of the solid residue, and, consequently, to an increase in its reactivity. The exposure of unburned carbon after complete extraction of glassy aluminosilicates may also have a place [59]. Previously, it was shown [59,60] that an alkali activation can further increase the specific surface area of the coal.

The liquor obtained by CFA leaching at suggested conditions can be used to precipitate mesoporous silica and zeolites, which are synthesized at similar L:S ratios [47]. The possibility of selective extraction of aluminum from the liquor and the solid residue will be discussed in future articles.

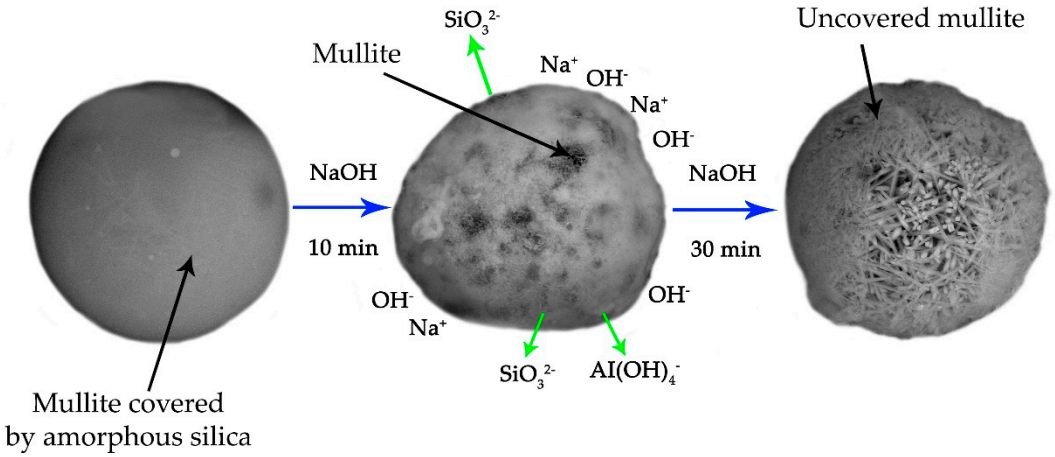

Figure 9. The mechanism of CFA desilication with the formation of acicular mullite particles.

4. Conclusions

In this article, the possibility of complete extraction of amorphous aluminosilicate from coal fly ash by alkali leaching under atmospheric pressure was studied. Using an artificial neural network method and the shrinking core model, it was shown that high L/S ratio and temperature is essential to increasing leaching efficiency. The main conclusion is as follows:

1. The raw CFA contains a large amount of amorphous aluminosilicate with high content of easily soluble alumina. The extraction of this alumina by the NaOH simultaneously with silica at low L/S ratio (<15) leads to the formation of DSP.
2. According to the response surfaces, at the T = 110 °C; C(Na_2O) = 400 g/L; L/S ratio = 20 and 60 min leaching duration, the Si and Al extraction degrees were 88% and 45%. A very low Na_2O content (0.65 mas.%) is observed in the solid residue at these conditions. It indicates the absence of the DSP formation.
3. The results of the kinetic analysis show that the leaching process is limited by the surface chemical reaction at low T <100 °C; at high T >100 °C—the leaching process is limited by the diffusion through the product layer. The apparent E_a was 73.8 kJ/mol.
4. Due to the NaOH leaching of CFA at conditions that prevent the formation of a DSP, mullite particles with an acicular structure are exposed. This leads to a significant increase of the porosity and specific surface area of the solid residue, and, consequently, to an increase in its reactivity.

Author Contributions: Conceptualization, I.L. and A.S.; methodology, I.L.; validation, L.C., I.L.; formal analysis, A.S., D.V.; investigation, L.C. and A.S.; resources, L.C., I.L.; data curation, I.L.; writing—original draft preparation, A.S., I.L.; writing—review and editing, A.S., D.V.; visualization, D.V.; supervision, A.S.; project administration, I.L.; funding acquisition, A.S. All authors have read and agreed to the published version of the manuscript.

Funding: This research was funded by Russian State Assignment, grant number 0836-2020-0020.

Acknowledgments: The authors would like to recognize the assistance provided by The Center for Collective Use Testing Analytical Center of the JSC "Scientific-research institute of chemical technology" and personally give thanks to Natalya Ognevskaya for the chemical analysis of solid and liquid samples. Authors also express our gratitude to Kolesnikov E. and Kondratiev A. from NUST MISiS for assistance on the SEM, XRD and BET analyses of solid samples and for English language editing, respectively.

Conflicts of Interest: The authors declare no conflict of interest.

References

1. Bazhin, V.Y.; Beloglazov, I.I.; Feshchenko, R.Y. Deep conversion and metal content of Russian coals. *Eurasian Min.* **2016**, *2*, 28–32. [CrossRef]
2. Yao, Z.T.; Xia, M.S.; Sarker, P.K.; Chen, T. A review of the alumina recovery from coal fly ash, with a focus in China. *Fuel* **2014**, *120*, 74–85. [CrossRef]
3. Dikhanbaev, B.; Dikhanbaev, A.B.; Sultan, I.; Rusowicz, A. Development of hydrogen-enriched water gas production technology by processing Ekibastuz coal with technogenic waste. *Arch. Mech. Eng.* **2018**. [CrossRef]
4. Bhatt, A.; Priyadarshini, S.; Acharath Mohanakrishnan, A.; Abri, A.; Sattler, M.; Techapaphawit, S. Physical, chemical, and geotechnical properties of coal fly ash: A global review. *Case Stud. Constr. Mater.* **2019**, *11*, e00263. [CrossRef]
5. Blissett, R.S.; Rowson, N.A. A review of the multi-component utilisation of coal fly ash. *Fuel* **2012**, *97*, 1–23. [CrossRef]
6. Coal Mining in Russia: Basic Indicators. Available online: https://minenergo.gov.ru/node/435 (accessed on 27 May 2020).
7. Ryabov, Y.V.; Delitsyn, L.M.; Ezhova, N.N.; Sudareva, S.V. Methods for Beneficiation of Ash and Slag Waste from Coal-Fired Thermal Power Plants and Ways for Their Commercial Use (a Review). *Therm. Eng.* **2019**, *66*, 149–168. [CrossRef]
8. Project Energy Strategy of the Russian Federation for the Period Until 2035. Available online: minenergo.gov.ru/node/1920 (accessed on 27 May 2020).

9. Amster, E. Public health impact of coal-fired power plants: A critical systematic review of the epidemiological literature. *Int. J. Environ. Health Res.* **2019**, 1–23. [CrossRef]
10. Ilic, M.; Cheeseman, C.; Sollars, C.; Knight, J. Mineralogy and microstructure of sintered lignite coal fly ash. *Fuel* **2003**, *82*, 331–336. [CrossRef]
11. Temimi, M.; Camps, J.P.; Laquerbe, M. Valorization of fly ash in the cold stabilization of clay materials. *Resour. Conserv. Recycl.* **1995**, *15*, 219–234. [CrossRef]
12. Manoharan, V.; Yunusa, I.A.M.; Loganathan, P.; Lawrie, R.; Skilbeck, C.G.; Burchett, M.D.; Murray, B.R.; Eamus, D. Assessments of Class F fly ashes for amelioration of soil acidity and their influence on growth and uptake of Mo and Se by canola. *Fuel* **2010**, *89*, 3498–3504. [CrossRef]
13. Matsi, T.; Keramidas, V.Z. Fly ash application on two acid soils and its effect on soil salinity, pH, B, P and on ryegrass growth and composition. *Environ. Pollut.* **1999**, *104*, 107–112. [CrossRef]
14. Lee, H.; Ha, H.S.; Lee, C.H.; Lee, Y.B.; Kim, P.J. Fly ash effect on improving soil properties and rice productivity in Korean paddy soils. *Bioresour. Technol.* **2006**, *97*, 1490–1497. [CrossRef] [PubMed]
15. Furlani, E.; Brückner, S.; Minichelli, D.; Maschio, S. Synthesis and characterization of ceramics from coal fly ash and incinerated paper mill sludge. *Ceram. Int.* **2008**, *34*, 2137–2142. [CrossRef]
16. Yao, Z.; Tan, S.; Xia, M.; Ye, Y.; Li, J. Synthesis, characterization and sintering behaviour of indialite ceramic from fly ash. *Waste Manag. Res.* **2011**, *29*, 1090–1097. [CrossRef]
17. Erol, M.; Küçükbayrak, S.; Ersoy-Meriçboyu, A. Characterization of sintered coal fly ashes. *Fuel* **2008**, *87*, 1334–1340. [CrossRef]
18. Erol, M.; Küçükbayrak, S.; Ersoy-Meriçboyu, A. Comparison of the properties of glass, glass–ceramic and ceramic materials produced from coal fly ash. *J. Hazard. Mater.* **2008**, *153*, 418–425. [CrossRef]
19. Xuan, X.; Yue, C.; Li, S.; Yao, Q. Selective catalytic reduction of NO by ammonia with fly ash catalyst. *Fuel* **2003**, *82*, 575–579. [CrossRef]
20. Jain, D.; Khatri, C.; Rani, A. Fly ash supported calcium oxide as recyclable solid base catalyst for Knoevenagel condensation reaction. *Fuel Process. Technol.* **2010**, *91*, 1015–1021. [CrossRef]
21. Saputra, E.; Muhammad, S.; Sun, H.; Ang, H.M.; Tadé, M.O.; Wang, S. Red mud and fly ash supported Co catalysts for phenol oxidation. *Catal. Today* **2012**, *190*, 68–72. [CrossRef]
22. Wang, S. Application of Solid Ash Based Catalysts in Heterogeneous Catalysis. *Environ. Sci. Technol.* **2008**, *42*, 7055–7063. [CrossRef]
23. Wang, S.; Wu, H. Environmental-benign utilisation of fly ash as low-cost adsorbents. *J. Hazard. Mater.* **2006**, *136*, 482–501. [CrossRef] [PubMed]
24. Hirajima, T.; Petrus, H.T.B.M.; Oosako, Y.; Nonaka, M.; Sasaki, K.; Ando, T. Recovery of cenospheres from coal fly ash using a dry separation process: Separation estimation and potential application. *Int. J. Miner. Process.* **2010**, *95*, 18–24. [CrossRef]
25. Niewiadomski, M.; Hupka, J.; Bokotko, R.; Miller, J.D. Recovery of coke fines from fly ash by air sparged hydrocyclone flotation. *Fuel* **1999**, *78*, 161–168. [CrossRef]
26. Shoumkova, A.S. Magnetic separation of coal fly ash from Bulgarian power plants. *Waste Manag. Res.* **2011**, *29*, 1078–1089. [CrossRef]
27. Valeev, D.; Kunilova, I.; Alpatov, A.; Mikhailova, A.; Goldberg, M.; Kondratiev, A. Complex utilisation of ekibastuz brown coal fly ash: Iron & carbon separation and aluminum extraction. *J. Clean. Prod.* **2019**, *218*, 192–201.
28. Verrecchia, G.; Cafiero, L.; de Caprariis, B.; Dell'Era, A.; Pettiti, I.; Tuffi, R.; Scarsella, M. Study of the parameters of zeolites synthesis from coal fly ash in order to optimize their CO_2 adsorption. *Fuel* **2020**, *276*, 118041. [CrossRef]
29. Ren, X.; Qu, R.; Liu, S.; Zhao, H.; Wu, W.; Song, H.; Zheng, C.; Wu, X.; Gao, X. Synthesis of Zeolites from Coal Fly Ash for Removal of Harmful Gaseous Pollutants: A Review. *Aerosol Air Qual. Res.* **2020**, *20*, 1127–1144. [CrossRef]
30. Liu, Z.; Li, S.; Li, L.; Wang, J.; Zhou, Y.; Wang, D. One-step high efficiency crystallization of zeolite A from ultra-fine circulating fluidized bed fly ash by hydrothermal synthesis method. *Fuel* **2019**, *257*, 116043. [CrossRef]
31. Malonda Shabani, J.; Babajide, O.; Oyekola, O.; Petrik, L. Synthesis of Hydroxy Sodalite from Coal Fly Ash for Biodiesel Production from Waste-Derived Maggot Oil. *Catalysts* **2019**, *9*, 1052. [CrossRef]

32. Torralvo, F.A.; Fernández-Pereira, C. Recovery of germanium from real fly ash leachates by ion-exchange extraction. *Miner. Eng.* **2011**, *24*, 35–41. [CrossRef]
33. Wang, N.; Sun, X.; Zhao, Q.; Yang, Y.; Wang, P. Leachability and adverse effects of coal fly ash: A review. *J. Hazard. Mater.* **2020**, *396*, 122725. [CrossRef] [PubMed]
34. Shi, Y.; Jiang, K.; Zhang, T.; Guo, J.; Zhao, A. Clean production of porous-Al(OH)3 from fly ash. *J. Hazard. Mater.* **2020**, *393*, 122371. [CrossRef] [PubMed]
35. Ding, J.; Ma, S.; Shen, S.; Xie, Z.; Zheng, S.; Zhang, Y. Research and industrialization progress of recovering alumina from fly ash: A concise review. *Waste Manag.* **2017**, *60*, 375–387. [CrossRef] [PubMed]
36. Valeev, D.; Shoppert, A.; Mikhailova, A.; Kondratiev, A. Acid and Acid-Alkali Treatment Methods of Al-Chloride Solution Obtained by the Leaching of Coal Fly Ash to Produce Sandy Grade Alumina. *Metals* **2020**, *10*, 585. [CrossRef]
37. Valeev, D.; Kunilova, I.; Shoppert, A.; Salazar-Concha, C.; Kondratiev, A. High-pressure HCl leaching of coal ash to extract Al into a chloride solution with further use as a coagulant for water treatment. *J. Clean. Prod.* **2020**, *276*, 123206. [CrossRef]
38. Ma, Z.; Zhang, S.; Zhang, H.; Cheng, F. Novel extraction of valuable metals from circulating fluidized bed-derived high-alumina fly ash by acid–alkali–based alternate method. *J. Clean. Prod.* **2019**, *230*, 302–313. [CrossRef]
39. Panek, R.; Wdowin, M.; Franus, W.; Czarna, D.; Stevens, L.A.; Deng, H.; Liu, J.; Sun, C.; Liu, H.; Snape, C.E. Fly ash-derived MCM-41 as a low-cost silica support for polyethyleneimine in post-combustion CO2 capture. *J. CO_2 Util.* **2017**, *22*, 81–90. [CrossRef]
40. Yan, F.; Jiang, J.; Tian, S.; Liu, Z.; Shi, J.; Li, K.; Chen, X.; Xu, Y. A Green and Facile Synthesis of Ordered Mesoporous Nanosilica Using Coal Fly Ash. *ACS Sustain. Chem. Eng.* **2016**, *4*, 4654–4661. [CrossRef]
41. Ju, T.; Jiang, J.; Meng, Y.; Yan, F.; Xu, Y.; Gao, Y.; Aihemaiti, A. An investigation of the effect of ultrasonic waves on the efficiency of silicon extraction from coal fly ash. *Ultrason. Sonochem.* **2020**, *60*, 104765. [CrossRef]
42. Kuppusamy, V.K.; Kumar, A.; Holuszko, M. Simultaneous Extraction of Clean Coal and Rare Earth Elements From Coal Tailings Using Alkali-Acid Leaching Process. *J. Energy Resour. Technol.* **2019**, *141*, 070708. [CrossRef]
43. Kumar, A.; Agrawal, S.; Dhawan, N. Processing of Coal Fly Ash for the Extraction of Alumina Values. *J. Sustain. Metall.* **2020**, *6*, 294–306. [CrossRef]
44. Guo, Y.; Zhao, Z.; Zhao, Q.; Cheng, F. Novel process of alumina extraction from coal fly ash by pre-desilicating—Na_2CO_3 activation—Acid leaching technique. *Hydrometallurgy* **2017**, *169*, 418–425. [CrossRef]
45. Bai, G.; Teng, W.; Wang, X.; Zhang, H.; Xu, P. Processing and kinetics studies on the alumina enrichment of coal fly ash by fractionating silicon dioxide as nano particles. *Fuel Process. Technol.* **2010**, *91*, 175–184. [CrossRef]
46. Smith, P. The processing of high silica bauxites—Review of existing and potential processes. *Hydrometallurgy* **2009**, *98*, 162–176. [CrossRef]
47. Czarna-Juszkiewicz, D.; Kunecki, P.; Panek, R.; Madej, J.; Wdowin, M. Impact of Fly Ash Fractionation on the Zeolitization Process. *Materials* **2020**, *13*, 1035. [CrossRef]
48. Kunecki, P.; Panek, R.; Wdowin, M.; Bień, T.; Franus, W. Influence of the fly ash fraction after grinding process on the hydrothermal synthesis efficiency of Na-A, Na-P1, Na-X and sodalite zeolite types. *Int. J. Coal Sci. Technol.* **2020**. [CrossRef]
49. Aphane, M.E.; Doucet, F.J.; Kruger, R.A.; Petrik, L.; van der Merwe, E.M. Preparation of Sodium Silicate Solutions and Silica Nanoparticles from South African Coal Fly Ash. *Waste Biomass Valor* **2019**. [CrossRef]
50. Shoppert, A.; Loginova, I.; Rogozhnikov, D.; Karimov, K.; Chaikin, L. Increased As Adsorption on Maghemite-Containing Red Mud Prepared by the Alkali Fusion-Leaching Method. *Minerals* **2019**, *9*, 60. [CrossRef]
51. Loginova, I.V.; Shoppert, A.A.; Chaikin, L.I. Effect of Adding Sintering Furnace Electrostatic Precipitator Dust on Combined Leaching of Bauxites and Cakes. *Metallurgist* **2015**, *59*, 698–704. [CrossRef]
52. Abdrakhimov, V.Z.; Abdrakhimova, E.S. Phase Structure of Pottery on the Basis of Waste Products of Combustible Slates, Coal Enrichment, Oil Extracting and Ashes Slag Materials. *Bull. Samara Sci. Cent. Russ. Acad. Sci.* **2013**, *15*, 82–95.

53. Xie, Y.; Wei, S.; Wang, X.; Xie, S.; Yang, C. A new prediction model based on the leaching rate kinetics in the alumina digestion process. *Hydrometallurgy* **2016**, *164*, 7–14. [CrossRef]
54. Shokri, A. Degradation of 4-Chloro phenol in aqueous media thru UV/Persulfate method by Artificial Neural Network and full factorial design method. *Int. J. Environ. Anal. Chem.* **2020**, 1–15. [CrossRef]
55. Myerson, A.S. *Handbook of Industrial Crystallization*; Butterworth-Heinemann: Oxford, UK, 2002; ISBN 978-0-08-053351-3.
56. Levenspiel, O. *Chemical Reaction Engineering*, 3rd ed.; Wiley: New York, NY, USA, 1999; ISBN 978-0-471-25424-9.
57. Taleb, K.; Markovski, J.; Milosavljević, M.; Marinović-Cincović, M.; Rusmirović, J.; Ristić, M.; Marinković, A. Efficient arsenic removal by cross-linked macroporous polymer impregnated with hydrous iron oxide: Material performance. *Chem. Eng. J.* **2015**, *279*, 66–78. [CrossRef]
58. Choo, T.F.; Mohd Salleh, M.A.; Kok, K.Y.; Matori, K.A.; Abdul Rashid, S. Characterization of High-Temperature Hierarchical Porous Mullite Washcoat Synthesized Using Aluminum Dross and Coal Fly Ash. *Crystals* **2020**, *10*, 178. [CrossRef]
59. Musyoka, N.M.; Wdowin, M.; Rambau, K.M.; Franus, W.; Panek, R.; Madej, J.; Czarna-Juszkiewicz, D. Synthesis of activated carbon from high-carbon coal fly ash and its hydrogen storage application. *Renew. Energy* **2020**, *155*, 1264–1271. [CrossRef]
60. Bazhin, V.Y. Structural modification of petroleum needle coke by adding lithium on calcining. *Coke Chem.* **2015**, *58*, 138–142. [CrossRef]